High-Pressure Synthesis of a B-site Co^{2+}/Mn^{4+} Disordered Quadruple Perovskite LaMn$_3$Co$_2$Mn$_2$O$_{12}$

Jia Guo, Xudong Shen, Zhehong Liu, Shijun Qin, Weipeng Wang, Xubin Ye, Guangxiu Liu, Richeng Yu, Hong-Ji Lin, Chien-Te Chen, Liu-Hao Tjeng, Zhiwei Hu, and Youwen Long*

Read Online

ACCESS | 📊 Metrics & More | 📖 Article Recommendations

ABSTRACT: A new oxide, LaMn$_3$Co$_2$Mn$_2$O$_{12}$, was synthesized under high-pressure (7 GPa) and high-temperature (1423 K) conditions. The compound crystallizes in an AA$'_3$B$_4$O$_{12}$-type quadruple perovskite structure with space group $Im\bar{3}$. The Rietveld structural analysis combined with soft X-ray absorption spectroscopy reveals the charge combination to be LaMn$^{3+}_3$Co$^{2+}_2$Mn$^{4+}_2$O$_{12}$, where the La^{3+} and Mn^{3+} are 1:3 ordered respectively at the A and A$'$ sites, whereas the Co^{2+} and Mn^{4+} are disorderly distributed at the B site. This is in sharp contrast to R$_2$Co^{2+}Mn^{4+}O$_6$ (R = La and rare earth) double perovskites, in which the Co^{2+} and Mn^{4+} charge states are always orderly distributed with a rocksalt-type fashion, giving rise to a long-range magnetic ordering. As a result, LaMn$_3$Co$_2$Mn$_2$O$_{12}$ displays spin glassy magnetic properties due to the random Co^{2+} and Mn^{4+} distribution, as demonstrated by dc and ac magnetic susceptibility as well as specific heat measurements. Possible factors that affect the B-site degree of order in perovskite structures are discussed.
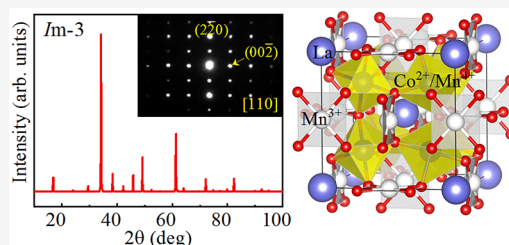
1. INTRODUCTION

Transition-metal (TM) oxides with perovskite and perovskite-related structures have received much attention owing to their diverse crystal structures and intriguing physical and chemical properties.[1−11] In a simple ABO$_3$ perovskite, the TM ions usually occupy the B site, dominating the electronic properties of the compound. Benefiting from the structure flexibility, one may get a B-site ordered A$_2$BB$'$O$_6$ double perovskite by appropriate substitution for the B site in a simple ABO$_3$ perovskite. The peculiar B−B$'$ interactions in double perovskites lead to a wide variety of interesting physical properties such as high-temperature ferro/ferrimagnetic half-metallicity,[12,13] magnetoelectric multiferroicity,[14] colossal magnetoresistance,[13,15] ferroelectric and piezoelectric effects, etc.[16−18] Recently, the family of R$_2$Co^{2+}Mn^{4+}O$_6$ manganite double perovskite has been studied widely because of their interesting magnetism and magnetodielectric properties.[19−31] Based on the Goodenough−Kanamori−Anderson (GKA) rules,[32−34] the ferromagnetic (FM) interaction is expected to occur between Co^{2+} and Mn^{4+} ions respectively with 3d^7(t$_{2g}^5$e$_g^2$) and 3d^3(t$_{2g}^3$) electronic configurations via the Co−O−Mn superexchange pathways, if the Co−O−Mn bond angle is close to 180°, whereas the antiferromagnetic (AFM) interaction will emerge if the bond angle is close to 90°. As shown in Figure 1, the magnetic phase diagram of R$_2$Co^{2+}Mn^{4+}O$_6$ family, when the A-site ionic size gradually decreases to reduce the Co−O−Mn bond angle, the FM Curie temperature (T_C) almost linearly decreases from 230 K in La$_2$CoMnO$_6$ (LCMO) with ∠Co−
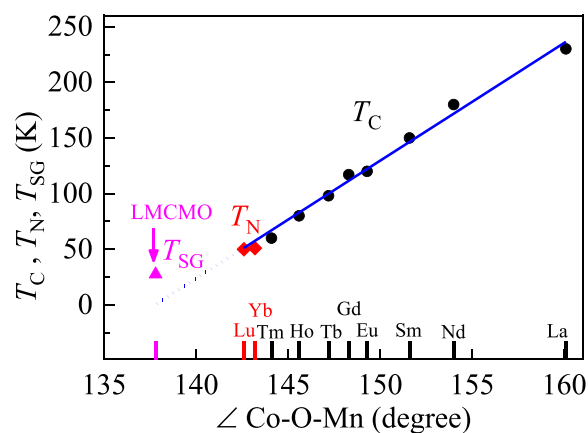
Figure 1. Magnetic transition temperature as a function of the average Co−O−Mn bond angle in the R$_2$CoMnO$_6$ family and LMCMO. T_C is the FM Curie temperature (black circles). T_N is the AFM Néel temperature (red diamonds), and T_{SG} is the spin glass transition temperature (magenta triangles). The blue line is a linear fitting for R$_2$CoMnO$_6$.
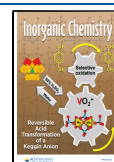
O−Mn = 160.1° to 60 K in Tm_2CoMnO_6 with ∠Co−O−Mn = 144.1°.[19,35] Further bending the bond angle to 143.2° for Yb and 142.6° for Lu, the E-type AFM ordering instead of the FM one takes place.[19] Moreover, a metamagnetic transition from the E-type AFM structure into a FM polarized structure is found to occur at higher magnetic field, suggesting a delicate balance between the AFM and FM interaction intensity in these two members.[19,20]

Compared with a rare earth, the TM has a much smaller ionic size. At ambient pressure, it is difficult to substitute a TM ion into the A site in a perovskite structure. Taking into account that high pressure can effectively modify the ionic size as well as the BO_6 octahedral distortion, the three-quarters of the A site can be substituted by a TM ion A′ and therefore an A-site ordered quadruple perovskite with chemical formula of $AA'_3B_4O_{12}$ can be formed under high pressure (see Figure 2a).[36] Furthermore, one may obtain a both A- and B-site
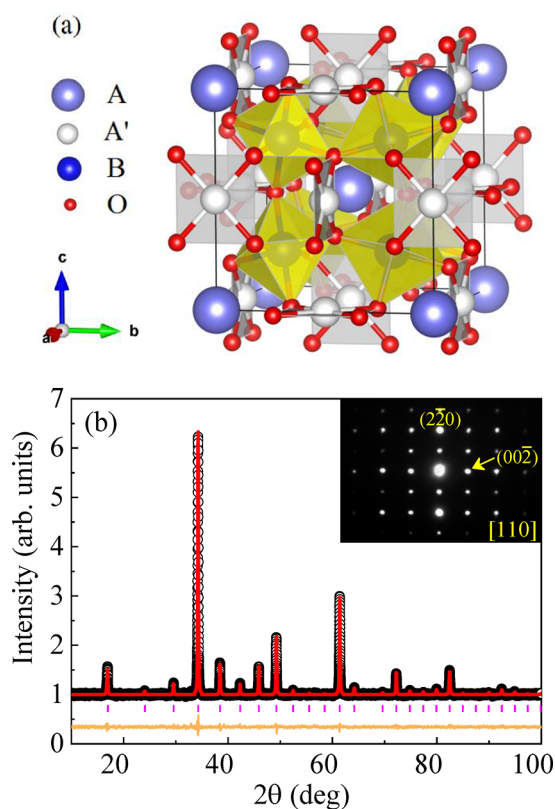
Figure 2. (a) Crystal structure of A-site ordered quadruple perovskite $AA'_3B_4O_{12}$ with $Im\overline{3}$ symmetry. The corner-sharing BO_6 octahedra and spatially isolated $A'O_4$ squares are shown. (b) XRD pattern collected at RT and the Rietveld refinement results for LMCMO. Observed (circles), calculated (red line), and difference (bottom line) profiles are shown. The magenta ticks indicate the allowed Bragg reflections with space group $Im\overline{3}$. The inset shows a SAED image along the [110] zone axis indicating Co/Mn disorder at the B site.

ordered quadruple perovskite $AA'_3B_2B'_2O_{12}$ via additional B-site substitution. To accommodate the average small A-site size, in these ordered quadruple perovskites, the B(B′)−O−B(B′) bond angle has to heavily tilt, so that a typical bond angle is bent to about 140°. Since multiple atomic sites (A′, B, and B′) accommodate TM ions, new magnetic and electrical interaction pathways (e.g., A′−A′ and A′−B/B′) that never occur in simple ABO_3 perovskites and B-site ordered double

perovskites show up in the quadruple perovskites.[37] As a consequence, a series of special emergent phenomena such as A′−B intersite charge transfer,[7,38−40] A- and B-site spins induced ferroelectricity,[8,11] and enhanced A′−B−B′ spin interactions with unusually high spin ordering temperatures are found to occur.[41,42] Recently, an A-site and B-site ordered quadruple perovskite oxide $LaMn_3Ni_2Mn_2O_{12}$(LMNMO) was reported.[43] Different from the relative double perovskite La_2NiMnO_6 which shows a single FM transition,[44] two distinct magnetic transitions take place in the quadruple one, where a G-type AFM ordering arising from the A′-site Mn^{3+} ions occurs at 46 K and then an orthogonal spin ordering contributed by the B-site Ni^{2+} and B′-site Mn^{4+} is observed at 34 K.[43] On account of the similar magnetic phase diagram between R_2NiMnO_6 and R_2CoMnO_6,[43] in this paper, a new oxide $LaMn_3Co_2Mn_2O_{12}$(LMCMO) with charge combination of $LaMn^{3+}_3Co^{2+}_2Mn^{4+}_2O_{12}$ was prepared by using high-pressure techniques. The crystal structure, valence state, magnetic, and specific heat properties are studied in detail. Unexpectedly, although all the $R_2Co^{2+}Mn^{4+}O_6$ members crystallize into a B-site ordered perovskite structure, the B-site Co^{2+} and Mn^{4+} are disorderly distributed in the current LMCMO, which is also in sharp contrast to the A- and B-site ordered $LaMn^{3+}_3Ni^{2+}_2Mn^{4+}_2O_{12}$.

2. EXPERIMENTAL DETAILS

The black polycrystalline LMCMO was synthesized from stoichiometric mixtures of highly pure (99.9%) La_2O_3, Mn_2O_3, CoO, and MnO_2 powders. The La_2O_3 powders were heated at 1273 K for 20 h before using. These reactants were thoroughly mixed and ground in an agate mortar and then pressed into a gold capsule with 3.0 mm in diameter and length within an argon-filled glovebox. The capsule was treated at 7 GPa and 1423 K for 30 min using a cubic-anvil-type high-pressure apparatus. After heating at 1423 K, the sample was slowly cooled to 1073 K within 5 h and then quenched to room temperature (RT). For comparison, another sample was quenched from 1423 K to RT. When the heating process was finished, the high pressure was slowly released to ambient in 6 h. For phase identification and crystal structure analysis, powder X-ray diffraction (XRD) was performed at RT on a Huber diffractometer (Cu−Kα1 radiation, 40 kV and 30 mA). The Rietveld analysis was performed to refine the crystallographic parameters using the GSAS program.[45] A Philips-CM200 field-emission transmission electron microscope with a field-emission gun manipulated at 200 keV was used to carried out high-resolution selected area electron diffraction (SAED) at RT along the [110] zone. The oxidation states of Mn and Co of LMCMO, together with $BiMn_3Cr_4O_{12}$ (BMCO), were studied by soft X-ray absorption spectroscopy (XAS) measurements at the beamline 11A of the National Synchrotron Radiation Research Center (NSRRC) in Taiwan. The $Mn-L_{2,3}$ and $Co-L_{2,3}$ XAS spectra of LMCMO were measured using the total electron yield (TEY) mode, and MnO and CoO single crystals were measured simultaneously as energy references for the $Mn-L_{2,3}$ and $Co-L_{2,3}$ edges, respectively. Magnetic susceptibility and magnetization were measured on a commercial superconducting quantum interference device magnetometer (MPMS3, Quantum Design). The magnetic susceptibility data were collected in zero-field-cooled (ZFC) and field-cooled (FC) modes in 2−300 K at a magnetic field of 0.1 T. The magnetic hysteresis loops at different temperatures of 300, 40, 20, and 2 K were measured between −7 and 7 T. A physical property measurement system (Quantum Design, PPMS7) was used to measure the frequency-dependent ac magnetization (M') and specific heat.

3. RESULTS AND DISCUSSION

The XRD pattern measured at RT as well as the related refinement results for the slow-cooled LMCMO sample are

presented in Figure 2b. All the diffraction peaks can be well identified as a cubic $AA'_3B_4O_{12}$-type quadruple perovskite structure with a space group $Im\bar{3}$, which is isostructural with $LaMn_3Cr_4O_{12}$.[8] No visible impurity phase is observed from the XRD pattern. In the $Im\bar{3}$ structural symmetry, the A-site La and A′-site Mn are distributed orderly in a rocksalt-type fashion with a ratio of 1:3, whereas the Co and Mn are arranged randomly at the B site. To further confirm the B-site Co/Mn disorder, the SAED was performed along the [110] zone axis for LMCMO. As shown in the inset of Figure 2b, the absence of any discernible diffraction spots with $h + k + l =$ odd, like the (111) spot, reveals the disordered distribution for Co/Mn at the B site,[46,47] in agreement with the XRD refinement. Table 1 lists the refined structural parameters,

Table 1. Refined Structure Parameters of LMCMO and the BVS Result for A′-site Mn at RT[a]

parameter	LMCMO
a (Å)	7.39303(1)
O_y	0.1743(3)
O_z	0.3098(2)
U_{iso}(La) $(100 \times Å^2)$	2.29(3)
U_{iso}(Mn$_{6b}$) $(100 \times Å^2)$	2.25(4)
U_{iso}(Co/Mn$_{8c}$) $(100 \times Å^2)$	2.16(3)
U_{iso}(O) $(100 \times Å^2)$	2.16(7)
Mn$_{6b}$-O $(\times 4$ Å)	1.907(1)
$(\times 4$ Å)	2.756(3)
$(\times 4$ Å)	3.307(3)
∠Co/Mn$_{8c}$−O−Co/Mn$_{8c}$ (deg)	137.8(1)
BVS (Mn$_{6b}$)	2.80
R_{wp} (%)	1.48
R_p (%)	1.11

[a]Space group: $Im\bar{3}$; atomic sites: La 2a (0, 0, 0), Mn 6b (0, 0.5, 0.5), Co/Mn 8c (0.25, 0.25, 0.25), O 24g (0, y, z). The BVS values (V_i) were calculated using the formula $V_i = \sum_j S_{ij}$, and $S_{ij} = \exp[(r_0 - r_{ij})/0.37]$. The value of $r_0 = 1.732$ for Mn$_{6b}$. For the Mn$_{6b}$, 12-coordinated oxygen atoms were used.

including lattice constant, atomic positions, selected bond lengths, and bond angles. Since Co^{2+} has a larger ionic radius compared with Ni^{2+},[48] the lattice parameter of LMCMO (7.39303 Å) is slightly larger than that of LMNMO (7.36863 Å) at RT. According to the A′-site Mn−O bond length, the bond valence sum (BVS) calculations give the valence state of Mn at this site is close to +3 (see Table 1). As Co and Mn randomly arrange, one cannot obtain the reliable valence states for these two TMs by the BVS method. Note that we analyzed the detailed crystal structure and magnetic susceptibility for both the slow-cooled and quenched LMCMO samples, and no visible difference is found to occur between them. Therefore, only the slow-cooled sample was used to show the related experimental results in this article.

It is well-known that the soft XAS at the 3d TM element $L_{2,3}$ edges are highly sensitive to their valence states[49−51] and local environment.[52−54] Figure 3a shows the Mn-$L_{2,3}$ XAS spectrum of LMCMO. For comparison, another A-site ordered quadruple perovskite $BiMn^{3+}_3Cr_4O_{12}$ was presented as a Mn^{3+} reference with a MnO_4 square coordination,[11] and a B-site ordered double perovskite $La_2Co^{2+}Mn^{4+}O_6$ was used as a Mn^{4+} reference with MnO_6 octahedral coordination.[21] Obviously, LMCMO shows a mixture from the A-site square-coordinated Mn^{3+} and B-site octahedral-coordinated
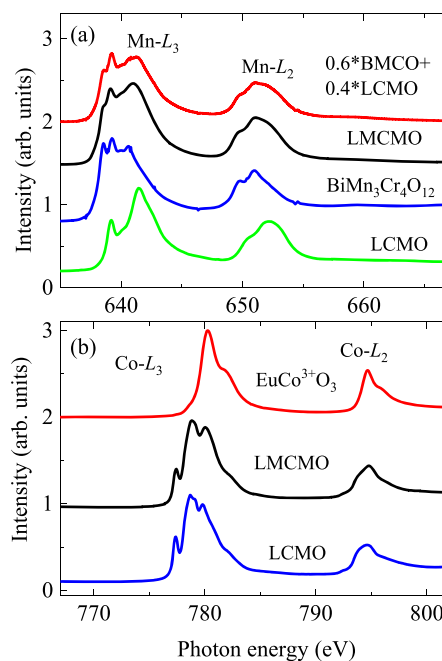
Figure 3. (a) The Mn-$L_{2,3}$ XAS spectra of LMCMO (black) with related references $BiMn^{3+}_3Cr_4O_{12}$ and $La_2CoMn^{4+}O_6$ (LMCO, green from ref 21). The red line stands for a simple superposition of BMCO and LMCO with a 3:2 ratio. (b) The Co-$L_{2,3}$XAS spectra of LMCMO (black) with related references LMCO and $EuCo^{3+}O_3$ from ref 55.

Mn^{4+}. Actually, the multiplet spectral feature as well as the peak energies of LMCMO can be well reproduced by a simple superposition of $BiMn^{3+}_3Cr_4O_{12}$ spectrum and LMCO spectrum with a 3:2 ratio, unveiling the formation of Mn^{3+} state at the A site and Mn^{4+} state at the B site.

The Co $L_{2,3}$-edges XAS of LMCMO is shown in Figure 3b, where the spectra of LMCO[21] and $EuCoO_3$ (from ref 55) are used as Co^{2+} and Co^{3+} references in octahedral coordination, respectively. One can see that, compared with the Co^{3+} reference $EuCoO_3$, the main peak of Co-L_3 edge of LMCMO shifts toward lower energy by about 1.5 eV but locates at the same energy of LMCO, demonstrating a Co^{2+} valence state. The very similar multiplet spectral feature of LMCO and LMCMO suggests also a very similar local environment of the Co ions. The XAS results thus confirm the charge combination and also local environments of Mn and Co ions in LMCMO to be $LaMn^{3+}_3Co^{2+}_2Mn^{4+}_2O_{12}$.

Since the A′-site Mn^{3+} and B-site Co^{2+} and Mn^{4+} are all magnetic ions, dc and ac magnetization measurements were performed to characterize the magnetism of LMCMO. Figure 4a shows the magnetic susceptibility curves measured in ZFC and FC modes at 0.1 T. Different from the double long-range spin orderings observed in LMNMO, only a single magnetic transition is found to occur in the current LMCMO at a critical temperature $T_{SG} \approx 27.5$ K. Moreover, there is a considerable separation between the ZFC and FC curves below T_{SG}. As shown by ac magnetization later, the magnetic transition is dependent on measurement frequency. Therefore, such a large ZFC and FC separation observed in the dc susceptibility is indicative of a spin glass transition. As reported in ref 21 on $LaMn^{4+}_{0.5}Co^{2+}_{0.5}O_3$, the Co^{2+} in octahedral coordination environment has a considerable contribution of orbital moment (0.99 μ_B/Co^{2+}), giving rise to the deviation of inverse susceptibility from the Curie−Weiss law at higher temper-
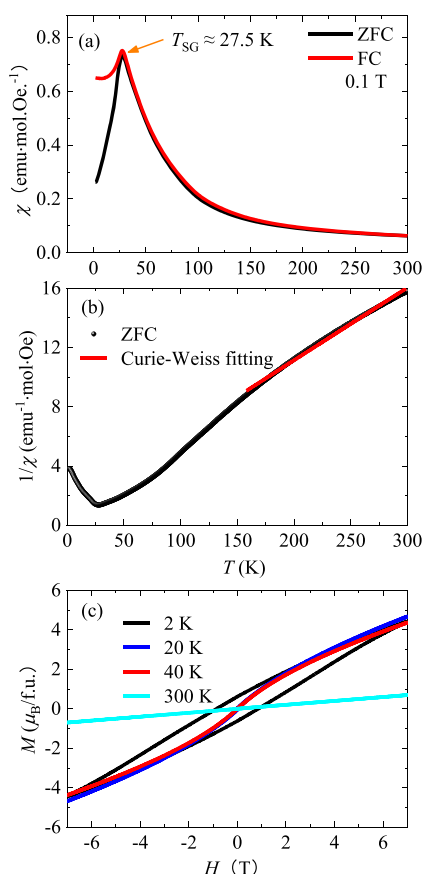
Figure 4. Temperature dependence of (a) dc magnetic susceptibility and (b) the inverse susceptibility measured at 0.1 T between 2 and 300 K for LMCMO. The red line in (b) shows the Curie−Weiss fitting above 155 K. (c) Isothermal magnetization curves measured at different temperatures.

atures. In analogy with $LaMn_{0.5}Co_{0.5}O_3$, the Co^{2+} in LMCMO may also have considerable orbital moment, so that the inverse susceptibility clearly deviates from the linear behavior below about 155 K, a temperature much higher than T_{SG}. Above 155 K, the inverse dc magnetic susceptibility follows the Curie−Weiss law with the function $\chi^{-1} = (T - \theta)/C$. The fitting result (shown by the red line in Figure 4b) gives a Curie constant C = 20.18 emu·K/mol and a Weiss temperature $\theta = -24.5$ K. Based on the Curie constant, the effective magnetic moment is calculated to be μ_{eff} = 12.71 μ_B/f.u., which is slightly larger than the spin-only theoretical value (11.49 μ_B/f.u.) for LMCMO with the charge format of $LaMn^{3+}_3Co^{2+}_2Mn^{4+}_2O_{12}$, probably due to the effect of orbital moment of Co^{2+}.

Figure 4c shows the isothermal magnetization curves measured at different temperatures for LMCMO. At the temperature well above T_{SG}, e.g., at 300 K, the linear magnetization behavior is coherent with the paramagnetism. At 40 K, the magnetization slightly deviates from the linear dependence on field without distinct magnetic hysteresis. It may imply the formation of some short-range FM correlations at the temperatures close to T_{SG}. Similar behaviors are observed in the isostructural spin-glass compounds $CaMn_3Fe_3MnO_{12}$ and $CaCu_3Mn_2Ir_2O_{12}$.[56,57] Below T_{SG} (e.g., at 2 K), however, one can find remarkable magnetic hysteresis as well as unsaturated magnetization behavior as the field increases to 7 T, suggesting the presence of competing FM and AFM interactions. The magnetization measurement thus

provides additional evidence for spin glass behavior of LMCMO.

To clarify the dynamic response for the spin glass transition of LMCMO, the ac magnetization was measured at 10 Oe and at different frequencies varying from 133 to 6333 Hz. As shown in Figure 5a, with increasing frequency, the cusp of ac
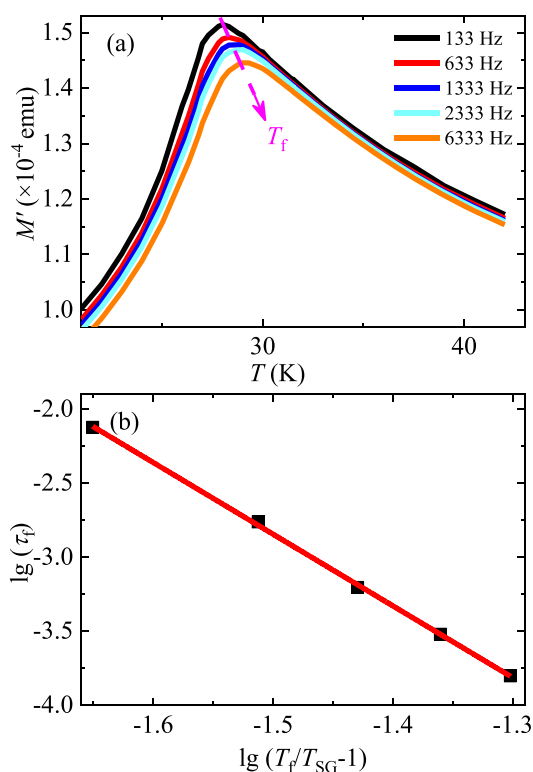
Figure 5. (a) Temperature dependence of ac magnetization measured at different frequencies. (b) The plot of $lg(\tau_f)$ vs $lg(T_f/T_{SG} - 1)$ and the fitting result (red line).

magnetization near T_{SG} shifts toward higher temperatures, accompanied with a reduction in magnitude. These features confirm the formation of the spin glass transition. To analyze the spin glass nature of LMCMO, the frequency dependence of freezing temperature T_f is depicted by a conventional dynamic scaling power law $\tau_f = \tau_0(T_f/T_{SG} - 1)^{-z\nu}$.[58] Here, $z\nu$ is the dynamical critical exponent, $\tau_f = 1/f$ is the microscopic spin relaxation time related to the measurement frequency f, and τ_0 is the characteristic relaxation time depending on the spin flipping time. This power law can be converted into the function $\ln(\tau_f) = \ln(\tau_0) - z\nu \ln(T_f/T_{SG} - 1)$. It means that a linear plot of $\ln(\tau_f)$ versus $\ln(T_f/T_{SG} - 1)$ is expected to be observed. Figure 5b shows the linear fitting, yielding τ_0 = 7.82(3) × 10^{-11} s and $z\nu$ = 4.84(5). The value of $z\nu$ is in accordance with the values of 4−12 reported in many canonical spin glass systems such as R_2NiSi_3 (R = Gd, Er) and $Eu_{0.5}Ba_{0.5}MnO_3$.[59,60] The value of τ_0 observed in LMCMO is also comparable with those reported in other spin glass systems with the magnitude ranging from 10^{-11} to 10^{-13} s.[56,58]

LMCMO exhibits high resistivity at RT (>10^5 Ω·cm), indicating the electrical insulating behavior due to the strong electron correlation effects at the Co^{2+} and Mn^{4+} sites. Figure 6 shows the temperature dependence of specific heat for LMCMO in the temperature range of 3−100 K. One cannot see a λ-type anomaly near T_{SG}, ruling out any long-range spin
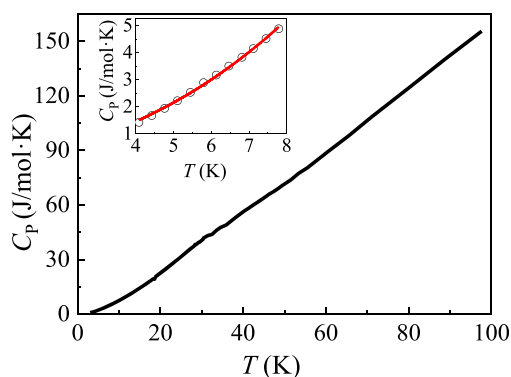
Figure 6. Temperature dependence of specific heat for LMCMO below 100 K at zero field. The inset shows the low-temperature fitting result between 4 and 8 K using the formula $C_P = \beta T^3 + \alpha T^{3/2}$.

ordering transition and agrees well with the nature of spin glass. As presented in the inset of Figure 6, at lower temperatures, the specific heat data can be fitted using the formula $C_P = \beta T^3 + \alpha T^{3/2}$,[61] where the T^3 term is attributed to phonon and short-range AFM contributions, while the $T^{3/2}$ term originates from the competing FM contribution. Because of the strong insulating behavior, no electronic contribution (proportional to T) is found to occur in specific heat. The coefficients were fitted to be $\beta = 3.34(4) \times 10^{-3}$ J/mol·K^4 and $\alpha = 1.55(1) \times 10^{-1}$ J/mol·K$^{5/2}$. Obviously, the value of α is much larger than that of β, illustrating that the competing FM contribution should dominate the specific heat.

We now discuss the origins of spin glass transition occurring in LMCMO. As is well-known, the magnetic properties of perovskites strongly depend on the B-site degree of order. In the current LMCMO, there exist magnetic A′-site Mn^{3+} and B-site Co^{2+}/Mn^{4+} ions. The Mn^{4+}(3d^3)−O−Mn^{4+}(3d^3) and Co^{2+}(3d^7)−O−Co^{2+}(3d^7) superexchange pathways will generate AFM interactions, while FM coupling is expected to occur via the Co^{2+}−O−Mn^{4+} superexchange pathway. Because of the disordered distribution of Co^{2+} and Mn^{4+}, competing AFM and FM interactions emerge. This is responsible for the presence of spin glass behavior. Note that, in some A-site ordered AMn$_3$B$_4$O$_{12}$ perovskites like YMn$_3$Al$_4$O$_{12}$,[62] La/BiMn$_3$Mn$_4$O$_{12}$,[63,64] and La/BiMn$_3$Cr$_4$O$_{12}$,[8,11] the A′-site Mn^{3+} ions can cause a long-range AFM transition. Even in the A-site ordered but B-site disordered CaMn$_3$(Fe$_3$Mn)O$_{12}$, the long-range AFM phase originating from the A′-site Mn^{3+} still exists at 39 K.[56] In the present LMCMO, however, one does not find any trace for A′-site Mn^{3+} spin ordering with temperature down to 2 K. We infer that the A′-site spin−spin interactions in LMCMO are correlated with B-site magnetic ions. This is reminiscent with the magnetic interactions as observed in LaMn$_3$Ni$^{2+}_2$Mn$^{4+}_2$O$_{12}$, where first-principles calculations indicate that the A′-site Mn^{3+} spins play a crucial role in determining the spin structure of the B-site Ni^{2+} and B′-site Mn^{4+}.[43]

We now turn to the magnetic phase diagram of R$_2$Co^{2+}Mn^{4+}O$_6$ double perovskite family shown in Figure 1. With decreasing Co−O−Mn bond angle (i.e., increasing octahedral distortion), although the magnetism changes from FM to AFM, the long-range magnetic transition temperature T_C or T_N almost shows a linear dependence from R = La to Lu. Compared with Lu$_2$CoMnO$_6$ which possesses the smallest Co−O−Mn bond angle (142.6°) in the R$_2$CoMnO$_6$ family,[19] the Co/Mn−O−Co/Mn bond angle observed in the current

LMCMO is further reduced to 137.8°. If the spin glass transition temperature of LMCMO is plotted in this phase diagram, it apparently deviates from the linear relationship mentioned above. In R$_2$CoMnO$_6$ family, the presence of Co^{2+} and Mn^{4+} always favors the formation of B-site order with a rocksalt-type fashion. Unexpectedly, although the Co^{2+} and Mn^{4+} charge states emerge in LMCMO, a B-site disordered perovskite structure is found to occur. In comparison, the crystal field between R$_2$CoMnO$_6$ and LMCMO is different. For example, in a single CoO$_6$ or MnO$_6$ octahedron in La$_2$CoMnO$_6$, there exist three different Co−O or Mn−O distances.[35] However, in the current LMCMO, the Co/MnO$_6$ octahedron is rigid. It means that one cannot distinguish the Co/Mn−O distances in macroscopy. In addition, the average Co−O−Mn bond angle of La$_2$CoMnO$_6$ (160.1°) is also significantly different from that of LMCMO (137.8°).[35] Therefore, the detailed crystal field which is closely related to BO$_6$ octahedral distortion probably can play a role to determine the B-site degree of order in a perovskite system, in addition to the well-known factors such as charge difference and ionic size difference.[65] Besides, during the sample synthesis, different heating processes can also affect the degree of B-site order. For example, in CaCu$_3$Fe$_2$Nb$_2$O$_{12}$, a slow-cooled method can form a higher Fe^{3+}/Nb^{5+} order structure, while a fast-cooled process leads to complete Fe^{3+}/Nb^{5+} disorder at the B site.[66] For the current LMCMO, however, the Co^{2+} and Mn^{4+} crystallize so far into a disordered perovskite structure regardless of the annealing or quenching heat treatment processes we used during synthesis. As mentioned in the Experimental Section, although the sample was slowly cooled from 1423 to 1073 K within 5 h, there is no trace for the formation of Co/Mn ordering in LMCMO. We speculate that it is difficult to prepare a Co/Mn ordered sample even using a longer-term high-pressure annealing process until to RT. It is also interesting to compare the distinct B-site construction between LaMn$^{3+}_3$Co$^{2+}_2$Mn$^{4+}_2$O$_{12}$ and LaMn$^{3+}_3$Ni$^{2+}_2$Mn$^{4+}_2$O$_{12}$. Although these two compounds have the same B-site charge difference and the ionic size difference of the former (Co^{2+} vs Mn^{4+}) is even slightly larger than that of the latter (Ni^{2+} vs Mn^{4+}), LMCMO crystallizes into a B-site disorder structure while an ordered one is found to occur in LMNMO when similar high-pressure synthesis method is used. This would be, on one hand, relative to the different chemical properties between Co^{2+} and Ni^{2+} ions, such as different electronic configuration and bonding behavior. In particular, the electron affinity between Co and Ni differs in a large degree. Specifically, the former is about 0.66 eV, while the latter is close to 1.16 eV. On the other hand, taking into account the different electronic configuration between Co^{2+} (t$_{2g}^5$e$_g^2$) with one unpaired t$_{2g}$ orbital and Ni^{2+} (t$_{2g}^6$e$_g^2$) with a fully occupied t$_{2g}$ orbital, distinct magnetic interactions originating from the A′−B intersite magnetic ions, i.e., Mn^{3+}−O−Co^{2+} superexchange interactions in LMCMO vs Mn^{3+}−O−Ni^{2+} ones in LMNMO, will occur. This may also affect the formation of the B-site disorderd structure with spin glass magnetic behavior in the current LMCMO. Anyway, LMCMO provides a unique example where Co^{2+} and Mn^{4+} show a robust disordered distribution in a perovskite-structure framework.

4. CONCLUSIONS

In summary, we have succeeded in preparing a new oxide LMCMO at high-pressure and high-temperature conditions.

XRD and SAED analyses confirm that the compound crystallizes in an A-site ordered but B-site disordered perovskite structure with $Im\bar{3}$ symmetry. The charge states based on the BVS calculations and XAS measurements are determined to be $LaMn^{3+}_3(Co^{2+}_2Mn^{4+}_2)O_{12}$, which is in agreement with the Curie−Weiss fitting. As revealed by dc and ac magnetization measurements, this B-site disordered perovskite shows a spin glass transition around 27.5 K due to the competing FM and AFM interactions generated by the randomly distributed Co^{2+} and Mn^{4+} magnetic ions. In sharp contrast to the B-site ordered double perovskite family of $R_2Co^{2+}Mn^{4+}O_6$, the current $LaMn^{3+}_3Co^{2+}_2Mn^{4+}_2O_{12}$ shows a disordered distribution for the B-site Co^{2+} and Mn^{4+} ions. In addition to the charge difference and ionic size difference, the detailed crystal chemistry correlated with the BO_6 octahedral distortion as well as the A′−B intersite magnetic interactions may also play roles on the degree of B-site order in perovskite-structure systems.

■ AUTHOR INFORMATION

Corresponding Author

Youwen Long − *Beijing National Laboratory for Condensed Matter Physics, Institute of Physics, Chinese Academy of Sciences, Beijing 100190, China; School of Physical Sciences, University of Chinese Academy of Sciences, Beijing 100049, China; Songshan Lake Materials Laboratory, Dongguan, Guangdong 523808, China;* ⊙ orcid.org/0000-0002-8587-7818; Email: ywlong@iphy.ac.cn

Authors

Jia Guo − *Beijing National Laboratory for Condensed Matter Physics, Institute of Physics, Chinese Academy of Sciences, Beijing 100190, China; School of Physical Sciences, University of Chinese Academy of Sciences, Beijing 100049, China*

Xudong Shen − *Beijing National Laboratory for Condensed Matter Physics, Institute of Physics, Chinese Academy of Sciences, Beijing 100190, China; Songshan Lake Materials Laboratory, Dongguan, Guangdong 523808, China*

Zhehong Liu − *Beijing National Laboratory for Condensed Matter Physics, Institute of Physics, Chinese Academy of Sciences, Beijing 100190, China; School of Physical Sciences, University of Chinese Academy of Sciences, Beijing 100049, China*

Shijun Qin − *Beijing National Laboratory for Condensed Matter Physics, Institute of Physics, Chinese Academy of Sciences, Beijing 100190, China; School of Physical Sciences, University of Chinese Academy of Sciences, Beijing 100049, China*

Weipeng Wang − *Beijing National Laboratory for Condensed Matter Physics, Institute of Physics, Chinese Academy of Sciences, Beijing 100190, China; School of Physical Sciences, University of Chinese Academy of Sciences, Beijing 100049, China*

Xubin Ye − *Beijing National Laboratory for Condensed Matter Physics, Institute of Physics, Chinese Academy of Sciences, Beijing 100190, China; School of Physical Sciences, University of Chinese Academy of Sciences, Beijing 100049, China*

Guangxiu Liu − *Beijing National Laboratory for Condensed Matter Physics, Institute of Physics, Chinese Academy of Sciences, Beijing 100190, China; School of Physical Sciences, University of Chinese Academy of Sciences, Beijing 100049, China*

Richeng Yu − *Beijing National Laboratory for Condensed Matter Physics, Institute of Physics, Chinese Academy of Sciences, Beijing 100190, China; School of Physical Sciences, University of Chinese Academy of Sciences, Beijing 100049, China*

Hong-Ji Lin − *National Synchrotron Radiation Research Center, Hsinchu 30076, Taiwan, R.O.C.*

Chien-Te Chen − *National Synchrotron Radiation Research Center, Hsinchu 30076, Taiwan, R.O.C.*

Liu-Hao Tjeng − *Max Planck Institute for Chemical Physics of Solids, Dresden 01187, Germany*

Zhiwei Hu − *Max Planck Institute for Chemical Physics of Solids, Dresden 01187, Germany*

Complete contact information is available at:
https://pubs.acs.org/10.1021/acs.inorgchem.0c01548

Notes
The authors declare no competing financial interest.

■ REFERENCES

(1) Cava, R. J.; Batlogg, B.; Vandover, R. B.; Murphy, D. W.; Sunshine, S.; Siegrist, T.; Remeika, J. P.; Rietman, E. A.; Zahurak, S.; Espinosa, G. P. Bulk superconductivity at 91 K in single-phase oxygen-deficient perovskite $Ba_2YCu_3O_{9-\delta}$. *Phys. Rev. Lett.* **1987**, *58*, 1676−1679.

(2) Dagotto, E.; Hotta, T.; Moreo, A. Colossal magnetoresistant materials: The key role of phase separation. *Phys. Rep.* **2001**, *344*, 1−153.

(3) Kimura, T.; Goto, T.; Shintani, H.; Ishizaka, K.; Arima, T.; Tokura, Y. Magnetic control of ferroelectric polarization. *Nature* **2003**, *426*, 55−58.

(4) Salamon, M. B.; Jaime, M. The physics of manganites: Structure and transport. *Rev. Mod. Phys.* **2001**, *73*, 583−628.

(5) Wang, J.; Neaton, J. B.; Zheng, H.; Nagarajan, V.; Ogale, S. B.; Liu, B.; Viehland, D.; Vaithyanathan, V.; Schlom, D. G.; Waghmare, U. V.; Spaldin, N. A.; Rabe, K. M.; Wuttig, M.; Ramesh, R. Epitaxial $BiFeO_3$ multiferroic thin film heterostructures. *Science* **2003**, *299*, 1719−1722.

(6) Homes, C. C.; Vogt, T.; Shapiro, S. M.; Wakimoto, S.; Ramirez, A. P. Optical response of high-dielectric-constant perovskite-related oxide. *Science* **2001**, *293*, 673−676.

(7) Long, Y. W.; Hayashi, N.; Saito, T.; Azuma, M.; Muranaka, S.; Shimakawa, Y. Temperature-induced A-B intersite charge transfer in an A-site-ordered $LaCu_3Fe_4O_{12}$ perovskite. *Nature* **2009**, *458*, 60−63.

(8) Wang, X.; Chai, Y. S.; Zhou, L.; Cao, H. B.; Cruz, C. D.; Yang, J. Y.; Dai, J. H.; Yin, Y. Y.; Yuan, Z.; Zhang, S. J.; Yu, R. Z.; Azuma, M.; Shimakawa, Y.; Zhang, H. M.; Dong, S.; Sun, Y.; Jin, C. Q.; Long, Y. W. Observation of Magnetoelectric Multiferroicity in a Cubic Perovskite System: $LaMn_3Cr_4O_{12}$. *Phys. Rev. Lett.* **2015**, *115*, 087601.

(9) Zeng, Z.; Greenblatt, M.; Subramanian, M. A.; Croft, M. Large low-field magnetoresistance in perovskite-type $CaCu_3Mn_4O_{12}$ without double exchange. *Phys. Rev. Lett.* **1999**, *82*, 3164−3167.

(10) Zhang, G.; Dong, S.; Yan, Z.; Guo, Y.; Zhang, Q.; Yunoki, S.; Dagotto, E.; Liu, J. M. Multiferroic properties of $CaMn_7O_{12}$. *Phys. Rev. B: Condens. Matter Mater. Phys.* **2011**, *84*, 174413.

(11) Zhou, L.; Dai, J. H.; Chai, Y. S.; Zhang, H. M.; Dong, S.; Cao, H. B.; Calder, S.; Yin, Y. Y.; Wang, X.; Shen, X. D.; Liu, Z. H.; Saito, T.; Shimakawa, Y.; Hojo, H.; Ikuhara, Y.; Azuma, M.; Hu, Z. W.; Sun, Y.; Jin, C. Q.; Long, Y. W. Realization of Large Electric Polarization

and Strong Magnetoelectric Coupling in BiMn$_3$Cr$_4$O$_{12}$. *Adv. Mater.* **2017**, *29*, 1703435.

(12) Kobayashi, K. I.; Kimura, T.; Tomioka, Y.; Sawada, H.; Terakura, K.; Tokura, Y. Intergrain tunneling magnetoresistance in polycrystals of the ordered double perovskite Sr$_2$FeReO$_6$. *Phys. Rev. B: Condens. Matter Mater. Phys.* **1999**, *59*, 11159–11162.

(13) Kobayashi, K. L.; Kimura, T.; Sawada, H.; Terakura, K.; Tokura, Y. Room-temperature magnetoresistance in an oxide material with an ordered double-perovskite structure. *Nature* **1998**, *395*, 677–680.

(14) Kim, M. K.; Moon, J. Y.; Oh, S. H.; Oh, D. G.; Choi, Y. J.; Lee, N. Strong magnetoelectric coupling in mixed ferrimagnetic-multiferroic phases of a double perovskite. *Sci. Rep.* **2019**, *9*, 5456.

(15) Ding, L.; Khalyavin, D. D.; Manuel, P.; Blake, J.; Orlandi, F.; Yi, W.; Belik, A. A. Colossal magnetoresistance in the insulating ferromagnetic double perovskites Tl$_2$NiMnO$_6$: A neutron diffraction study. *Acta Mater.* **2019**, *173*, 20–26.

(16) Azuma, M.; Takata, K.; Saito, T.; Ishiwata, S.; Shimakawa, Y.; Takano, M. Designed ferromagnetic, ferroelectric Bi$_2$NiMnO$_6$. *J. Am. Chem. Soc.* **2005**, *127*, 8889–8892.

(17) De, C.; Arevalo-Lopez, A. M.; Orlandi, F.; Manuel, P.; Attfield, J. P.; Sundaresan, A. Isovalent Cation Ordering in the Polar Rhombohedral Perovskite Bi$_2$FeAlO$_6$. *Angew. Chem., Int. Ed.* **2018**, *57*, 16099–16103.

(18) Sun, L.; Fang, Y.-W.; He, J.; Zhang, Y.; Qi, R.; He, Q.; Huang, R.; Xiang, P.; Tang, X.-D.; Yang, P.; Chu, J.; Chu, Y.-H.; Duan, C.-G. The preparation, and structural and multiferroic properties of B-site ordered double-perovskite Bi$_2$FeMnO$_6$. *J. Mater. Chem. C* **2017**, *5*, 5494–5500.

(19) Blasco, J.; Garcia-Munoz, J. L.; Garcia, J.; Subias, G.; Stankiewicz, J.; Rodriguez-Velamazan, J. A.; Ritter, C. Magnetic order and magnetoelectric properties of R$_2$CoMnO$_6$ perovskites (R = Ho, Tm, Yb, and Lu). *Phys. Rev. B: Condens. Matter Mater. Phys.* **2017**, *96*, 024409.

(20) Blasco, J.; García-Muñoz, L.; García, J.; Stankiewicz, J.; Subías, G.; Ritter, C.; Rodríguez-Velamazán, J. A. Evidence of large magnetodielectric effect coupled to a metamagnetic transition in Yb$_2$CoMnO$_6$. *Appl. Phys. Lett.* **2015**, *107*, 012902.

(21) Burnus, T.; Hu, Z.; Hsieh, H. H.; Joly, V. L. J.; Joy, P. A.; Haverkort, M. W.; Wu, H.; Tanaka, A.; Lin, H. J.; Chen, C. T.; Tjeng, L. H. Local electronic structure and magnetic properties of LaMn$_{0.5}$Co$_{0.5}$O$_3$ studied by x-ray absorption and magnetic circular dichroism spectroscopy. *Phys. Rev. B: Condens. Matter Mater. Phys.* **2008**, *77*, 125124.

(22) Dass, R. I.; Goodenough, J. B. Multiple magnetic phases of La$_2$CoMnO$_{6-\delta}$ ($0 \leq \delta \leq 0.05$). *Phys. Rev. B: Condens. Matter Mater. Phys.* **2003**, *67*, 014401.

(23) Jia, Y.; Wang, Q.; Wang, P.; Li, L. Structural, magnetic and magnetocaloric properties in R$_2$CoMnO$_6$ (R = Dy, Ho, and Er). *Ceram. Int.* **2017**, *43*, 15856–15861.

(24) Jia, Y. S.; Li, Y.; Zhao, L. Z.; Li, L. W. Magnetism and critical behavior of double perovskite RE$_2$CoMnO$_6$ (RE = La and Eu) compounds. *J. Magn. Magn. Mater.* **2019**, *481*, 156–161.

(25) Kim, M. K.; Moon, J. Y.; Choi, H. Y.; Oh, S. H.; Lee, N.; Choi, Y. J. Investigation of the magnetic properties in double perovskite R$_2$CoMnO$_6$ single crystals (R = rare earth: La to Lu). *J. Phys.: Condens. Matter* **2015**, *27*, 426002.

(26) Silva, R. X.; Almeida, R. M.; Moreira, R. L.; Paniago, R.; Rezende, M. V. S.; Paschoal, C. W. A. Vibrational properties and infrared dielectric features of Gd$_2$CoMnO$_6$ and Y$_2$CoMnO$_6$ double perovskites. *Ceram. Int.* **2019**, *45*, 4756–4762.

(27) Silva, R. X.; de Menezes, A. S.; Almeida, R. M.; Moreira, R. L.; Paniago, R.; Marti, X.; Reichlova, H.; Marysko, M.; Rezende, M. V. d. S.; Paschoal, C. W. A. Structural order, magnetic and intrinsic dielectric properties of magnetoelectric La$_2$CoMnO$_6$. *J. Alloys Compd.* **2016**, *661*, 541–552.

(28) Silva, R. X.; Moreira, R. L.; Almeida, R. M.; Paniago, R.; Paschoal, C. W. A. Intrinsic dielectric properties of magnetodielectric La$_2$CoMnO$_6$. *J. Appl. Phys.* **2015**, *117*, 214105.

(29) Singh, M. P.; Truong, K. D.; Fournier, P. Magnetodielectric effect in double perovskite La$_2$CoMnO$_6$ thin films. *Appl. Phys. Lett.* **2007**, *91*, 042504.

(30) Yang, D. X.; Yang, T.; Chen, Y. L.; Liang, Y.; Liu, Y. G. Ferromagnetism, structure transitions, and strain coupling of magnetoelastic double perovskite La$_2$CoMnO$_6$. *J. Mater. Sci.* **2019**, *54*, 6027–6037.

(31) Yang, W. Z.; Liu, X. Q.; Zhao, H. J.; Chen, X. M. Magnetic, dielectric and transport characteristics of Ln$_2$CoMnO$_6$ (Ln = Nd and Sm) double perovskite ceramics. *J. Magn. Magn. Mater.* **2014**, *371*, 52–59.

(32) Anderson, P. W. Antiferromagnetism - Theory of Superexchange Interaction. *Phys. Rev.* **1950**, *79*, 350–356.

(33) Goodenough, J. B. Theory of the Role of Covalence in the Perovskite-Type Manganites [LA, M(II)] MnO$_3$. *Phys. Rev.* **1955**, *100*, 564–573.

(34) Kanamori, J. Superexchange Interaction and Symmetry Properties of Electron Orbitals. *J. Phys. Chem. Solids* **1959**, *10*, 87–98.

(35) Viswanathan, M; Anil Kumar, P S; Bhadram, V. S.; Narayana, C.; Bera, A K; Yusuf, S M Influence of lattice distortion on the Curie temperature and spin-phonon coupling in LaMn$_{0.5}$Co$_{0.5}$O$_3$. *J. Phys.: Condens. Matter* **2010**, *22*, 346006.

(36) Vasil'ev, A. N.; Volkova, O. S. New functional materials AC$_3$B$_4$O$_{12}$ (Review). *Low Temp. Phys.* **2007**, *33*, 895–914.

(37) Long, Y. A-site ordered quadruple perovskite oxides AA′$_3$B$_4$O$_{12}$. *Chin. Phys. B* **2016**, *25*, 078108.

(38) Long, Y.; Saito, T.; Tohyama, T.; Oka, K.; Azuma, M.; Shimakawa, Y. Intermetallic Charge Transfer in A-Site-Ordered Double Perovskite BiCu$_3$Fe$_4$O$_{12}$. *Inorg. Chem.* **2009**, *48*, 8489–8492.

(39) Long, Y.; Shimakawa, Y. Intermetallic charge transfer between A-site Cu and B-site Fe in A-site-ordered double perovskites. *New J. Phys.* **2010**, *12*, 063029.

(40) Yamada, I.; Shiro, K.; Etani, H.; Marukawa, S.; Hayashi, N.; Mizumaki, M.; Kusano, Y.; Ueda, S.; Abe, H.; Irifune, T. Valence Transitions in Negative Thermal Expansion Material SrCu$_3$Fe$_4$O$_{12}$. *Inorg. Chem.* **2014**, *53*, 10563–10569.

(41) Chen, W.-T.; Mizumaki, M.; Seki, H.; Senn, M. S.; Saito, T.; Kan, D.; Attfield, J. P.; Shimakawa, Y. A half-metallic A- and B-site-ordered quadruple perovskite oxide CaCu$_3$Fe$_2$Re$_2$O$_{12}$ with large magnetization and a high transition temperature. *Nat. Commun.* **2014**, *5*, 3909.

(42) Deng, H.; Liu, M.; Dai, J.; Hu, Z.; Kuo, C.; Yin, Y.; Yang, J.; Wang, X.; Zhao, Q.; Xu, Y.; Fu, Z.; Cai, J.; Guo, H.; Jin, K.; Pi, T.; Soo, Y.; Zhou, G.; Cheng, J.; Chen, K.; Ohresser, P.; Yang, Y.-f.; Jin, C.; Tjeng, L.-H.; Long, Y. Strong enhancement of spin ordering by A-site magnetic ions in the ferrimagnet CaCu$_3$Fe$_2$Os$_2$O$_{12}$. *Phys. Rev. B: Condens. Matter Mater. Phys.* **2016**, *94*, 024414.

(43) Yin, Y. Y.; Liu, M.; Dai, J. H.; Wang, X.; Zhou, L.; Cao, H. B.; dela Cruz, C.; Chen, C. T.; Xu, Y. J.; Shen, X.; Yu, R. C.; Alonso, J. A.; Munoz, A.; Yang, Y. F.; Jin, C. Q.; Hu, Z. W.; Long, Y. W. LaMn$_3$Ni$_2$Mn$_2$O$_{12}$: An A- and B-Site Ordered Quadruple Perovskite with A-Site Tuning Orthogonal Spin Ordering. *Chem. Mater.* **2016**, *28*, 8988–8996.

(44) Rogado, N. S.; Li, J.; Sleight, A. W.; Subramanian, M. A. Magnetocapacitance and magnetoresistance near room temperature in a ferromagnetic semiconductor: La$_2$NiMnO$_6$. *Adv. Mater.* **2005**, *17*, 2225–2227.

(45) Larson, A. C.; Von Dreele, R. B. General Structure Analysis System (GSAS). *Report No. LAUR 86-748*; Los Alamos National Laboratory: Los Alamos, NM, 1994.

(46) Byeon, S. H.; Lee, S. S.; Parise, J. B.; Woodward, P. M.; Hur, N. H. High-Pressure Synthesis of Metallic Perovskite Ruthenate CaCu$_3$Ga$_2$Ru$_2$O$_{12}$. *Chem. Mater.* **2004**, *16*, 3697–3701.

(47) Byeon, S. H.; Lee, S. S.; Parise, J. B.; Woodward, P. M.; Hur, N. H. New Ferrimagnetic Oxide CaCu$_3$Cr$_2$Sb$_2$O$_{12}$: High-Pressure Synthesis, Structure, and Magnetic Properties. *Chem. Mater.* **2005**, *17*, 3552–3557.

(48) Shannon, R. D. Revised Effective Ionic Radii and Systematic Studies of Interatomic Distances in Halides and Chalcogenides. *Acta*

Crystallogr., Sect. A: Cryst. Phys., Diffr., Theor. Gen. Crystallogr. **1976**, *32*, 751−767.

(49) Mitra, C.; Hu, Z.; Raychaudhuri, P.; Wirth, S.; Csiszar, S. I.; Hsieh, H. H.; Lin, H. J.; Chen, C. T.; Tjeng, L. H. Direct observation of electron doping in $La_{0.7}Ce_{0.3}MnO_3$ using x-ray absorption spectroscopy. *Phys. Rev. B: Condens. Matter Mater. Phys.* **2003**, *67*, 092404.

(50) Pellegrin, E.; Tjeng, L. H.; deGroot, F. M. F.; Hesper, R.; Sawatzky, G. A.; Moritomo, Y.; Tokura, Y. Soft X-ray magnetic circular dichroism study of the colossal magnetoresistance compound $La_{1-x}Sr_xMnO3$. *J. Electron Spectrosc. Relat. Phenom.* **1997**, *86*, 115−118.

(51) Vasiliev, A. N.; Volkova, O. S.; Lobanovskii, L. S.; Troyanchuk, I. O.; Hu, Z.; Tjeng, L. H.; Khomskii, D. I.; Lin, H. J.; Chen, C. T.; Tristan, N.; Kretzschmar, F.; Klingeler, R.; Buechner, B. Valence states and metamagnetic phase transition in partially B-site-disordered perovskite $EuMn_{0.5}Co_{0.5}O_3$. *Phys. Rev. B: Condens. Matter Mater. Phys.* **2008**, *77*, 104442.

(52) Hollmann, N.; Hu, Z.; Willers, T.; Bohaty, L.; Becker, P.; Tanaka, A.; Hsieh, H. H.; Lin, H. J.; Chen, C. T.; Tjeng, L. H. Local symmetry and magnetic anisotropy in multiferroic $MnWO_4$ and antiferromagnetic $CoWO_4$ studied by soft x-ray absorption spectroscopy. *Phys. Rev. B: Condens. Matter Mater. Phys.* **2010**, *82*, 184429.

(53) Burnus, T.; Hu, Z.; Wu, H.; Cezar, J. C.; Niitaka, S.; Takagi, H.; Chang, C. F.; Brookes, N. B.; Lin, H. J.; Jang, L. Y.; Tanaka, A.; Liang, K. S.; Chen, C. T.; Tjeng, L. H. X-ray absorption and x-ray magnetic dichroism study on Ca_3CoRhO_6 and Ca_3FeRhO_6. *Phys. Rev. B: Condens. Matter Mater. Phys.* **2008**, *77*, 205111.

(54) Hollmann, N.; Agrestini, S.; Hu, Z.; He, Z.; Schmidt, M.; Kuo, C. Y.; Rotter, M.; Nugroho, A. A.; Sessi, V.; Tanaka, A.; Brookes, N. B.; Tjeng, L. H. Spectroscopic evidence for exceptionally high orbital moment induced by local distortions in α-CoV_2O_6. *Phys. Rev. B: Condens. Matter Mater. Phys.* **2014**, *89*, 201101.

(55) Hu, Z.; Wu, H.; Haverkort, M. W.; Hsieh, H. H.; Lin, H. J.; Lorenz, T.; Baier, J.; Reichl, A.; Bonn, I.; Felser, C.; Tanaka, A.; Chen, C. T.; Tjeng, L. H. Different look at the spin state of Co^{3+} ions in a CoO_5 pyramidal coordination. *Phys. Rev. Lett.* **2004**, *92*, 207402.

(56) Guo, J.; Ye, X.; Liu, Z.; Wang, W.; Qin, S.; Zhou, B.; Hu, Z.; Lin, H.-J.; Chen, C.-T.; Yu, R.; Tjeng, L. H.; Long, Y. High-pressure synthesis of A-site ordered perovskite $CaMn_3(Fe_3Mn)O_{12}$ and sequential long-range antiferromagnetic ordering and spin glass transition. *J. Solid State Chem.* **2019**, *278*, 120921.

(57) Ye, X.; Liu, Z.; Wang, W.; Hu, Z.; Lin, H.-J.; Weng, S.-C.; Chen, C.-T.; Yu, R.; Tjeng, L.-H.; Long, Y. High-pressure synthesis and spin glass behavior of a Mn/Ir disordered quadruple perovskite $CaCu_3Mn_2Ir_2O_{12}$. *J. Phys.: Condens. Matter* **2020**, *32*, 075701.

(58) Binder, K.; Young, A. P. Spin Glasses: Experimental Facts, Theoretical Concepts, and Open Questions. *Rev. Mod. Phys.* **1986**, *58*, 801−976.

(59) Pakhira, S.; Mazumdar, C.; Ranganathan, R.; Giri, S.; Avdeev, M. Large magnetic cooling power involving frustrated antiferromagnetic spin-glass state in R_2NiSi_3 (R = Gd, Er). *Phys. Rev. B: Condens. Matter Mater. Phys.* **2016**, *94*, 104414.

(60) Mathieu, R.; Akahoshi, D.; Asamitsu, A.; Tomioka, Y.; Tokura, Y. Colossal magnetoresistance without phase separation: Disorder-induced spin glass state and nanometer scale orbital-charge correlation in half doped manganites. *Phys. Rev. Lett.* **2004**, *93*, 4227202.

(61) Anand, V. K.; Adroja, D. T.; Hillier, A. D. Ferromagnetic cluster spin-glass behavior in $PrRhSn_3$. *Phys. Rev. B: Condens. Matter Mater. Phys.* **2012**, *85*, 014418.

(62) Tohyama, T.; Saito, T.; Mizumaki, M.; Agui, A.; Shimakawa, Y. Antiferromagnetic interaction between A'-site Mn spins in A-site-ordered perovskite $YMn_3Al_4O_{12}$. *Inorg. Chem.* **2010**, *49*, 2492−2495.

(63) Imamura, N.; Karppinen, M.; Motohashi, T.; Fu, D.; Itoh, M.; Yamauchi, H. Positive and Negative Magnetodielectric Effects in A-Site Ordered $(BiMn_3)Mn_4O_{12}$ Perovskite. *J. Am. Chem. Soc.* **2008**, *130*, 14948−14949.

(64) Prodi, A.; Allodi, G.; Gilioli, E.; Licci, F.; Marezio, M.; Bolzoni, F.; Gauzzi, A.; De Renzi, R. μSR study of $AA'_3Mn_4O_{12}$ double perovskites. *Phys. B* **2006**, *374*, 55−58.

(65) Vasala, S.; Karppinen, M. $A_2B'B''O_6$ perovskites: A review. *Prog. Solid State Chem.* **2015**, *43*, 1−36.

(66) Senn, M. S.; Chen, W.-t.; Saito, T.; Garcia-Martin, S.; Attfield, J. P.; Shimakawa, Y. B-Cation Order Control of Magnetism in the 1322 Perovskite $CaCu_3Fe_2Nb_2O_{12}$. *Chem. Mater.* **2014**, *26*, 4832−4837.